

## Supporting Information

### **Two-dimensional lead-free iodide-based hybrid double perovskites: crystal growth, thin-film preparation and photocurrent responses**

Le-Yu Bi,<sup>a,‡</sup> Yue-Qiao Hu,<sup>b,‡</sup> Mu-Qing Li,<sup>a</sup> Tian-Li Hu,<sup>a</sup> Hao-Lan Zhang,<sup>a</sup> Xing-Tian Yin,<sup>c</sup>  
Wen-Xiu Que,<sup>c</sup> Mohamed Saber Lassoued,<sup>a</sup> and Yan-Zhen Zheng<sup>\*a</sup>

---

a. Frontier Institute of Science and Technology (FIST), Shenzhen Research School, State Key Laboratory for Mechanical Behavior of Materials, MOE Key Laboratory for Nonequilibrium Synthesis of Condensed Matter, Xi'an Key Laboratory of Sustainable Energy and Materials Chemistry and School of Science, Xi'an Jiaotong University, Xi'an, Shaanxi 710054, P. R. China E-mail: zheng.yanzhen@xjtu.edu.cn

b. Key Laboratory of Advanced Molecular Engineering Materials, Baoji University of Arts and Sciences, No. 1 Hi-Tec Avenue, Baoji 721013, P. R. China.

c. Electronic Materials Research Laboratory, Key Laboratory of the Ministry of Education, International Center for Dielectric Research, School of Electronic & Information Engineering, Xi'an Jiaotong University, Xi'an 710049, Shaanxi, P. R. China.

[‡] These authors contributed equally to this work

## Experimental Section

### General remarks

All reagents and solvents for the syntheses were purchased from commercial sources and used without further purification. PXRD intensities were measured at 293 K on a Rigaku D/max-III A diffractometer (Cu-K $\alpha$ ,  $\lambda$  = 1.54056 Å). The crystalline powder samples were prepared by grinding the single-crystals and scanned from 2 theta = 5° to 60° at a rate of 10 °/min.

### Syntheses of the compounds.

Red crystals of (NH<sub>3</sub>C<sub>6</sub>H<sub>10</sub>NH<sub>3</sub>)<sub>2</sub>AgBiI<sub>8</sub>·H<sub>2</sub>O (**AgBiI**) (Figure S1 (a)) were obtained from hydrothermal reaction of BiI<sub>3</sub> (1 mmol), Ag<sub>2</sub>O (0.5 mmol), *cis*-1,4-cyclohexanediamine (2.0 mmol), and aqueous hydrogen iodide (5 mL, 55 % wt) at 160 °C for 6 hours. The crystals of **AgBiI** were washed with ethanol and dried in vacuum (Yield: *ca.* 91 % based on Bi). XRD indicates the phase purity (Figure S4 (a)).

Black crystals of (NH<sub>3</sub>C<sub>6</sub>H<sub>10</sub>NH<sub>3</sub>)<sub>2</sub>CuBiI<sub>8</sub>·0.5H<sub>2</sub>O (**CuBiI**) (Figure S1(b)) were synthesized from a similar method. A mixture of BiI<sub>3</sub> (1.0 mmol), CuI (1.0 mmol) and *trans*-1,4-cyclohexanediamine (2.0 mmol) were added to 5 mL aqueous hydrogen iodide (55 % wt), then the reaction solutions were heated at 160 °C for 6 hours. The crystals of **CuBiI** were washed with ethanol and dried in vacuum (Yield *ca.* 86 % for **CuBiI**, based on Bi). XRD indicates the phase purity (Figure S4 (b)).

Yellow crystals of Cs<sub>2</sub>AgBiBr<sub>6</sub> (Figure S1 (c)) were obtained from a similar method. A mixture of Bi<sub>2</sub>O<sub>3</sub> (0.5 mmol), Ag<sub>2</sub>O (0.5 mmol) and Cs<sub>2</sub>CO<sub>3</sub> (1.0 mmol) were added to 5 mL aqueous hydrogen bromide (48 % wt), then the reaction solutions were heated at 160 °C for 6 hours. The crystals of Cs<sub>2</sub>AgBiBr<sub>6</sub> were washed with ethanol and dried in vacuum (Yield *ca.* 40 % based on Bi). XRD indicates the phase purity (Figure S4 (c)).

**X-ray Crystallography.** Single-crystal X-ray diffraction data collections for **AgBiI** and **CuBiI** were conducted on a Bruker SMART APEX II CCD diffractometer (Mo,  $\lambda$  = 0.71073 Å) by using the  $\theta$ - $\omega$  scan technique at 150 K. The structures were solved by

direct methods and refined with a full-matrix least-squares technique within the SHELXTL program package.<sup>[1]</sup> All non-hydrogen atoms were refined anisotropically. The crystallographic details are provided in Table S1, S2, S3. Crystallographic data for the structural analyses have been deposited at the Cambridge Crystallographic Data Centre. The crystallographic data for above compounds can be found in the Supporting Information or can be obtained free of charge from the Cambridge Crystallographic Data Centre via [http://www.ccdc.cam.ac.uk/data\\_request/cif](http://www.ccdc.cam.ac.uk/data_request/cif). CCDC Numbers: 1900561 (**AgBiI**), 1900574 (**CuBiI**).

**Two-point probe conductivity measurements.** For electrical measurements, the two ends of the single crystals were connected to a source meter (Keithley 2400). The silver coated copper wire was used as the conductor wire, and conductive silver paste was used to stick the wire and the crystals. Current-voltage ( $I$ - $V$ ) curves were scanned at various voltage ranges according to the resistance of the single crystals and the sensitivity of the instrument. The conductivity is calculated by the plots of current density versus electric field strength ( $J$ - $E$  curves) based on the following Ohm's law,

$$\sigma = J / E,$$

$$J = I / S,$$

$$E = V / L$$

where  $\sigma$  is the conductivity,  $J$  is the current density,  $E$  is the electric field strength,  $I$  is the current,  $V$  is the voltage,  $S$  is the cross-sectional area of the pressed pellets, and  $L$  is the thickness of the pellets.

**Optical measurements.** Solid-state UV-Vis diffusion reflectance spectra of pressed powder samples or films were measured on a SHIMADZU UV-3600 UV-Vis-NIR spectrophotometer using BaSO<sub>4</sub> powder as the reflectance reference. The absorption spectra were calculated from reflectance spectra by the Kubelka-Munk function:  $F(R) = \alpha/S = (1-R)^2/2R$ , where  $R$ ,  $\alpha$ , and  $S$  are the coefficients for the reflection, the absorption and the scattering, respectively.

The absorption onsets of films blue shifted from those of powder samples for the same compound. We thought this related to the size of the compound. Instead of quantum confinement effect, we found scattering and absorption of incident light are causes of size dependent color change of **AgBiI** and **CuBiI**. The relationship between color and particle size is well studied according to Mie scattering in many fields, and the pigment is one of the fields that related to this topic. As Dimitrije Radjenović et al. reported, after grinding, several colored materials (like copper(II) sulfate pentahydrate, cobalt(II) chloride hexahydrate, brown rosin and yellow rosin) get more light colors close to white.<sup>[2]</sup> Such phenomena are studied by many groups, they all owe the size dependent color change to the Mie scattering.<sup>[3-5]</sup> Not only in the mineral pigments but also in the hybrid perovskite was this phenomena discovered. Karunadasa et al. reported the absorption spectra of  $(\text{BA})_4\text{AgBiBr}_8$ ,  $(\text{BA})_2\text{CsAgBiBr}_8$ ,  $\text{Cs}_2\text{AgBiBr}_6$  films all blue shifted than powder samples.<sup>[6]</sup> No matter for the film or the loose powder, complex surface morphology will introduce much scattering on crystal boundaries. So only after excluding the scattering can we obtain the intrinsic optical properties. One way is to test the UV-vis spectrum on single crystal, and another is to test on the pressed pellet which excludes the air among the particles and has a smooth surface. So we considered the absorption onsets of pressed powder rather than that of films as the band gaps.

**Photoluminescence measurement.** Room-temperature steady-state emission spectra were collected on powder samples using an Edinburgh FLS9 fluorimeter upon 530 nm excitation. Because the weak emission spectra were affected by noise, 600 nm filter was used to reduce the noise.

**Computational methods.** All density-functional theory (DFT) calculations were carried out within the Materials Studio. The crystallographic data of compound **AgBiI** or **CuBiI** was used to calculate the electronic band structures and the densities of the states (DOSs) without further optimization. The ab initio calculations of the band structure, DOS and PDOS were performed using the CASTEP. The exchange-correlation energy was calculated using Perdew-Burke-Ernzerhof (PBE) modification to the generalized gradient approximation (GGA).<sup>[7]</sup> The convergence threshold for the

self-consistent field was  $10^{-6}$  Ha. The Brillouin zone has been sampled with a highly-converged set of k points, using grids up to  $(4 \times 6 \times 4)$  points according to the Monkhorst Pack scheme<sup>[8]</sup> for all calculations.

The DFT calculation of **AgBiI** band structure were executed with or without SOC in an elastic compute servicer with 12 cores and 96 GB memory. When excluding the spin orbit coupling (SOC), the kinetic energy cutoff we used was 260 eV with ultrasoft pseudopotentials. For the case of including the SOC, we applied norm conserving pseudopotentials and the kinetic energy cutoff was 600 eV. Excluding SOC, the result shows an indirect band gap of 2.28 eV between valence band maximum (VBM) G and conduction band minimum (CBM) D (Figure S5 (a)). When SOC was included, the calculated band gap was still indirect, but the CBM shifted from D to Z and the bandgap decreased to 1.53 eV (Figure S5 (b)). The predicted band gaps including or excluding SOC are both different from experiment results for more than 350 meV. PDOS figures of AgBiI show that near the band gap (-2 to 3 eV) the DOS is mainly contributed by inorganic part (Figure S5 (c)) and indicate that the VBM is primarily contributed by I p and Ag d orbitals, whereas the CBM is mainly derived from Bi p , I p orbitals in Figure S5 (d).

The calculation of CuBiI with or without SOC were executed in a servicer of 12 cores and 96 GB memory . When excluding the spin orbit coupling (SOC), the kinetic energy cutoff we used was 600 eV with norm conserving pseudopotentials. For the case of including the SOC, we applied norm conserving pseudopotentials and the kinetic energy cutoff was 870 eV. But calculations were failed for running out of memory which were due to the larger cell volume of CuBiI. In the program feedback information, the estimated memory for band structure calculation exceed 120 GB. While for the program including the SOC, the SCF could not lower than  $10^{-5}$  eV/atom to achieve convergence in the geometrical optimization program. And we estimate that more than 500 GB memory will be required in the band structure calculation.

**Film fabrication.** The film is fabricated through spin-coating dehydrate DMF/DMSO

or dehydrate DMF solution of **AgBiI** or **CuBiI** on an unheated ITO-glass substrate, which is followed by annealing on a hot plate in air at 70 °C. Film thickness can be adjusted by controlling solution concentration, spin-coating speed and accelerate speed. Here we obtained 250 nm thick films with solution of 0.25 g/mL, spin-coating speed of 1000 rpm and accelerate speed of 1000 rpm/s, and the spin-coating process maintained 60 s to insure the film uniformity. The film quality related to the crystallization process, which highly related with the annealing temperature. Here different annealing processes were performed. With one step 70 °C annealing for 10 min we got uniform films with less pin holes, and the color changing process from yellow to red-brown happened in 15-25 s.

**Photo response measurement.** Pellets of pressed powder of CuBiI and AgBiI were used for the photo response measurement (Figure S7). We use silver paint to make current collectors and to attach the silver-clad copper wires. The areas of silver paint are two semicircles, and one narrow strip like area was left without paint which can receive light from the lamp. Since the resistance in this system is as high as about  $10^{11}$   $\Omega$ , contact resistances between pellet sample, silver paint and wires are negligible. For that reason, two-probe measurements were adopted. We used a picoammeter (Keithley 6485) in series with a source meter (Keithley 2400) to detect the small current in this test. A 350 W solar-simulating Xenon lamp was used as light source. For every 60 s we blocked or unblocked the light and detected the current change. The current was so small that we have to use a high bias voltage (40 V) to separate the signals from the noise of the system.

**Table S1** Summary of crystal data and structural refinements

	<b>AgBiI</b>	<b>CuBiI</b>
CCDC number	1900561	1900574
Empirical formula	C <sub>12</sub> H <sub>34</sub> AgBi <sub>8</sub> N <sub>4</sub> O	C <sub>12</sub> H <sub>33</sub> BiCuI <sub>8</sub> N <sub>4</sub> O <sub>0.5</sub>
Formula weight	1582.48	1529.14
Crystal system	monoclinic	monoclinic
Space group	P2 <sub>1</sub> /n	P2 <sub>1</sub> /n
<i>a</i> /Å	8.556(6)	17.062(6)
<i>b</i> /Å	19.504(15)	19.825(7)
<i>c</i> /Å	19.181(14)	18.808(7)
$\alpha$ /°	90	90
$\beta$ /°	93.488(11)	90.297(5)
$\gamma$ /°	90	90
Volume/Å <sup>3</sup>	3195(4)	6362(4)
<i>Z</i>	4	8
$\rho$ calcg/cm <sup>3</sup>	3.290	3.193
$\mu$ /mm <sup>-1</sup>	13.856	13.968
F(000)	2784.0	5384
Reflections collected	29824	56482
Independent reflections	6327 [R <sub>int</sub> = 0.0963, R <sub>sigma</sub> = 0.0792]	13153 [R <sub>int</sub> = 0.0592, R <sub>sigma</sub> = 0.0533]
Data/restraints/parameters	6327/10/251	13153/0/484
Goodness-of-fit on F <sup>2</sup>	1.031	1.026
Final R indexes [I >= 2 $\sigma$ (I)]	R <sub>1</sub> = 0.0982, wR <sub>2</sub> = 0.2395	R <sub>1</sub> = 0.0438, wR <sub>2</sub> = 0.0880
Final R indexes [all data]	R <sub>1</sub> = 0.1455, wR <sub>2</sub> = 0.2743	R <sub>1</sub> = 0.0686, wR <sub>2</sub> = 0.0974

**Table S2** Summary of selected bond lengths (Å) and band angles (°) of **AgBiI**.

<b>Bond</b>	<b>Lengths / Å</b>	<b>Bond pair</b>	<b>Angles / °</b>	<b>Bond pair</b>	<b>Angles / °</b>
Bi1-I1	3.044(3)	I1-Bi1-I3	89.70(6)	I5-Bi1-I3	174.49(6)
Bi1-I3	3.072(3)	I1-Bi1-I2	88.41(7)	I5-Bi1-I2	87.31(6)
Bi1-I4	3.030(3)	I1-Bi1-I6	178.54(7)	I5-Bi1-I6	91.00(7)
Bi1-I2	3.101(3)	I3-Bi1-I2	87.23(5)	I6-Bi1-I3	90.08(7)
Bi1-I5	3.044(3)	I4-Bi1-I1	90.31(8)	I6-Bi1-I2	93.02(8)
Bi1-I6	3.058(3)	I4-Bi1-I3	92.17(6)	Ag1-I6-Bi1	163.10(13)
I7-Ag1	2.686(4)	I4-Bi1-I2	178.59(6)	I7-Ag1-I6	103.24(12)
I8-Ag1	2.683(4)	I4-Bi1-I5	93.27(6)	I8-Ag1-I7	149.75(17)
I6-Ag1	2.970(4)	I4-Bi1-I6	88.25(8)	I8-Ag1-I6	106.34(12)
		I5-Bi1-I1	89.35(6)		

**Table S3** Summary of selected bond lengths (Å) and band angles (°) of **CuBiI**

<b>Bond</b>	<b>Lengths / Å</b>	<b>Bond pair</b>	<b>Angles / °</b>	<b>Bond pair</b>	<b>Angles / °</b>
Bi1-I2	3.1095(11)	I2-Bi1-I16 <sup>1</sup>	93.54(3)	I9-Bi2-I12	176.36(2)
Bi1-I6	3.1944(12)	I2-Bi1-I4	86.78(2)	I9-Bi2-I10	90.79(2)
Bi1-I4	3.1748(13)	I4-Bi1-I16 <sup>1</sup>	86.71(2)	I9-Bi2-I8	89.27(2)
Bi1-I3	2.9842(13)	I3-Bi1-I2	89.82(2)	I9-Bi2-I13	95.91(2)
Bi1-I5	3.0317(11)	I3-Bi1-I16 <sup>1</sup>	95.78(2)	I9-Bi2-I11	91.65(2)
Bi1-I1	2.9353(11)	I3-Bi1-I4	175.91(3)	I11-Bi2-I12	91.20(2)
Bi2-I12	3.1917(14)	I3-Bi1-I5	90.99(2)	I11-Bi2-I10	85.96(3)
Bi2-I10	3.0174(11)	I5-Bi1-I2	177.37(2)	I11-Bi2-I8	175.15(2)
Bi2-I8	3.1598(12)	I5-Bi1-I16 <sup>1</sup>	83.88(4)	I11-Bi2-I13	92.32(3)
Bi2-I13	3.1294(12)	I5-Bi1-I4	92.50(2)	Cu1-I8-Bi2	152.72(5)
Bi2-I9	2.9849(13)	I1-Bi1-I2	95.11(4)	Cu2-I13-Bi2	154.88(4)
Bi2-I11	2.9940(11)	I1-Bi1-I16 <sup>1</sup>	168.79(3)	Cu2-I16-Bi12	143.07(5)
I8-Cu1	2.7784(19)	I1-Bi1-I4	86.68(2)	Cu1-I5-Bi1	158.82(4)
I6-Cu1	2.5781(19)	I1-Bi1-I3	91.36(2)	I14-Cu2-I13	96.64(6)
I14-Cu2	2.5900(19)	I1-Bi1-I5	87.38(4)	I14-Cu2-I16	103.18(6)
I7-Cu1	2.5530(19)	I10-Bi2-I12	87.15(2)	I16-Cu2-I13	103.73(7)
I13-Cu2	3.005(2)	I10-Bi2-I8	89.27(3)	I15-Cu2-I14	141.68(8)
I16-Bi12	3.1944(12)	I10-Bi2-I13	173.14(2)	I15-Cu2-I13	100.13(6)
I16-Cu2	2.6875(18)	I8-Bi2-I12	87.71(2)	I15-Cu2-I16	105.87(6)
I15-Cu2	2.5456(18)	I13-Bi2-I12	86.24(2)		
I5-Cu1	2.906(2)	I13-Bi2-I8	92.32(3)		

<sup>1</sup>1/2+X,3/2-Y,1/2+Z; <sup>2</sup>-1/2+X,3/2-Y,-1/2+Z; <sup>3</sup>1-X,1-Y,1-Z; <sup>4</sup>-X,1-Y,1-Z; <sup>5</sup>1-X,1-Y,2-Z; <sup>6</sup>-X,1-Y,2-Z

**Table S4** Photoelectric response for **AgBiI** and **CuBiI** at  $\pm 40$  V under 350 W xenon lamp irradiation.

compound	$I_{\text{light}}(+)$ (nA)	$I_{\text{dark}}(+)$ (nA)	$I_{\text{light}}/I_{\text{dark}}(+)$	$I_{\text{light}}(-)$ (nA)	$I_{\text{dark}}(-)$ (nA)	$I_{\text{light}}/I_{\text{dark}}(-)$
<b>AgBiI</b>	7.92	0.184	43.0	7.25	0.164	44.2
<b>CuBiI</b>	0.834	0.0286	29.2	0.756	0.0271	27.9

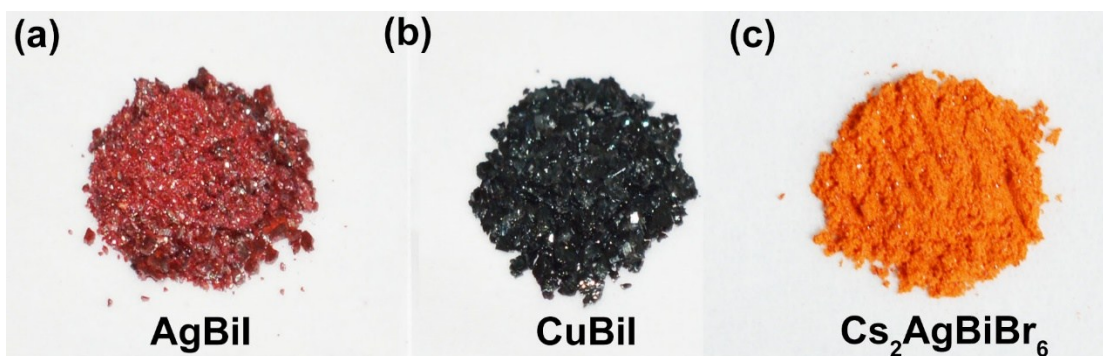


**Figure S1.** The crystal images of (a) **AgBiI** (red crystals), (b) **CuBiI** (black crystals) and (c) **Cs<sup>2</sup>AgBiBr<sub>6</sub>** (yellow crystals).

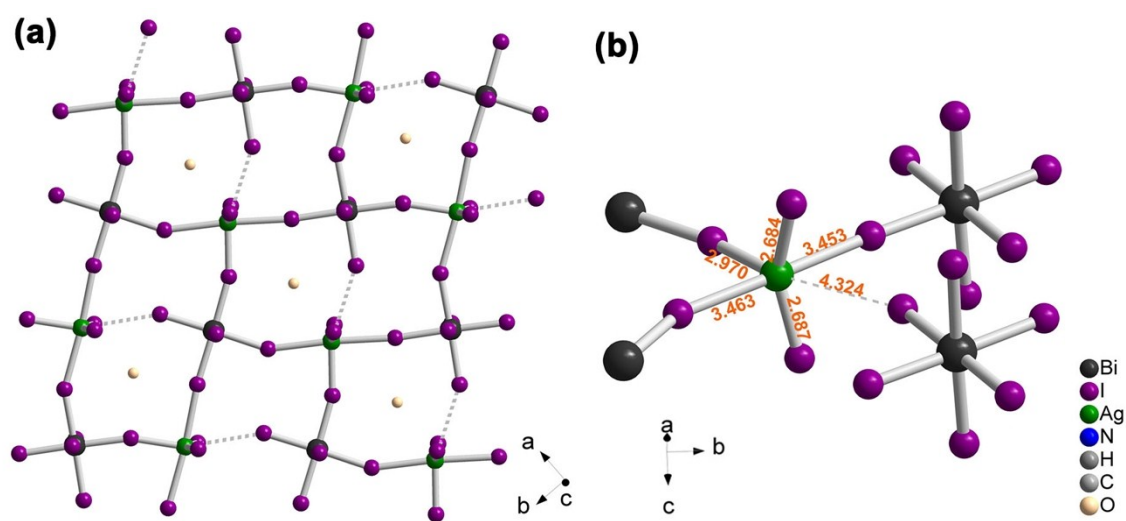


**Figure S2.** The 2D layered structure of **AgBiI**.

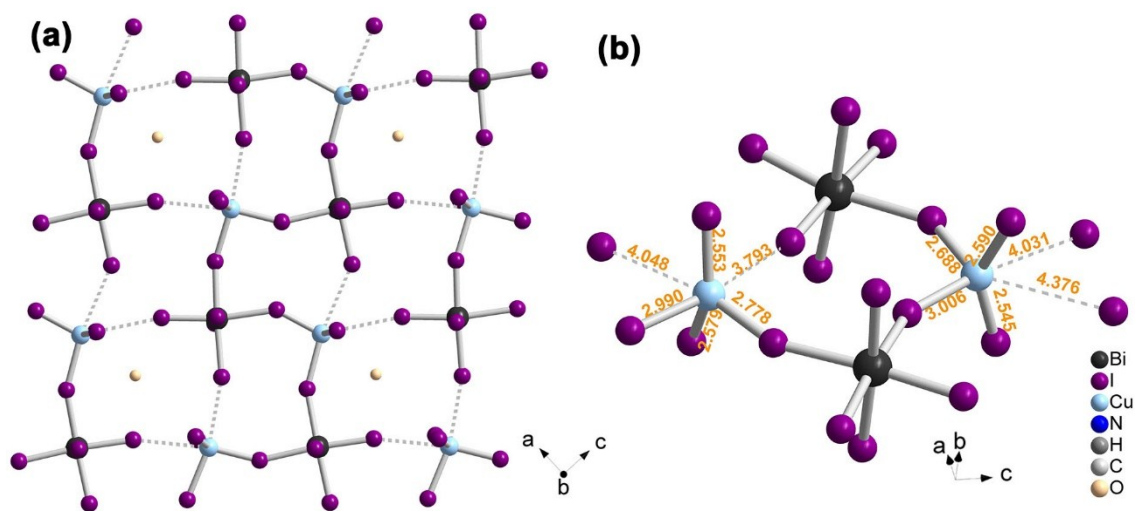


**Figure S3.** The 2D layered structure of **CuBiI**.

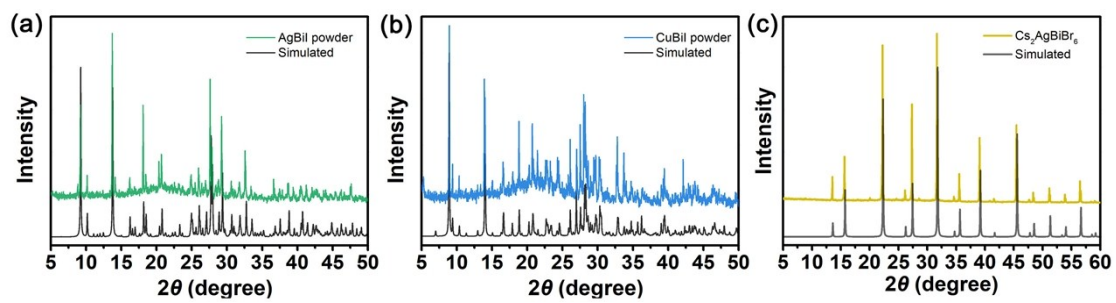


**Figure S4.** XRD patterns of **AgBiI** (a), **CuBiI** (b) and **Cs<sub>2</sub>AgBiBr<sub>6</sub>** indicate the phases purity.

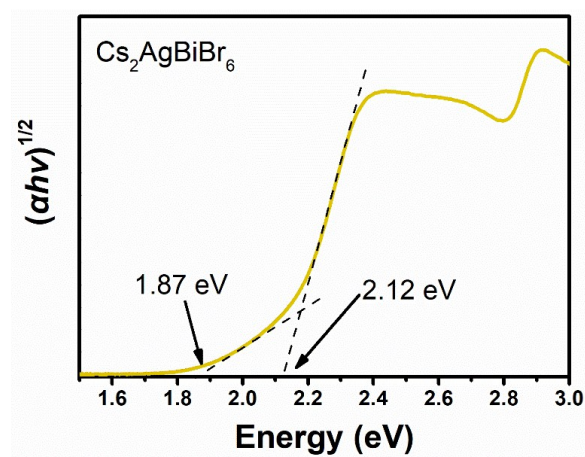


**Figure S5.** Tauc plot of powder sample of **Cs<sub>2</sub>AgBiBr<sub>6</sub>** with transitions at 1.87 eV and 2.12 eV.

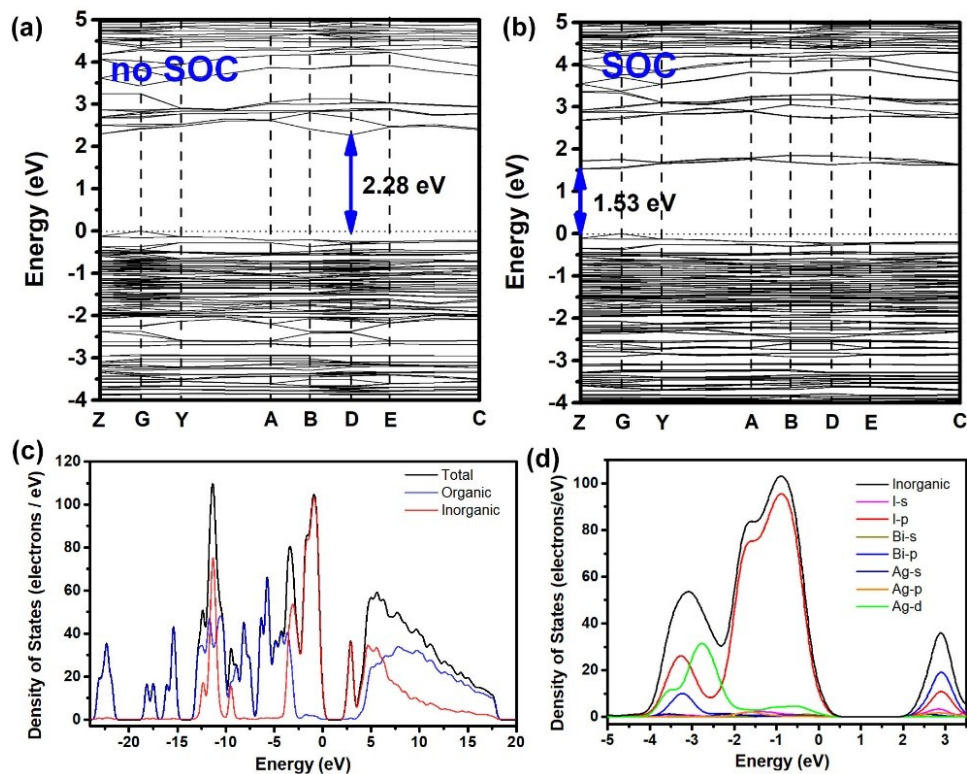


**Figure S6.** (a) GGA-PBE band structure of **AgBiI** excluding SOC. (b) GGA-PBE band structure of **AgBiI** including SOC. (c) Partial density of states (PDOS) for organic part and inorganic part, and total density of states (TDOS) of **AgBiI**. Near the band gap (-2 to 3 eV), the DOS is mainly contributed by inorganic part. (d) Partial density of states (PDOS) of inorganic part, I-*s*, I-*p*, Bi-*s*, Bi-*p*, Ag-*s*, Ag-*p* and Ag-*d*. The valence band maximum (VBM) is primarily contributed by I *p* and Ag *d* orbitals, whereas the conduction band minimum (CBM) is mainly derived from Bi *p*, I *p* orbitals.

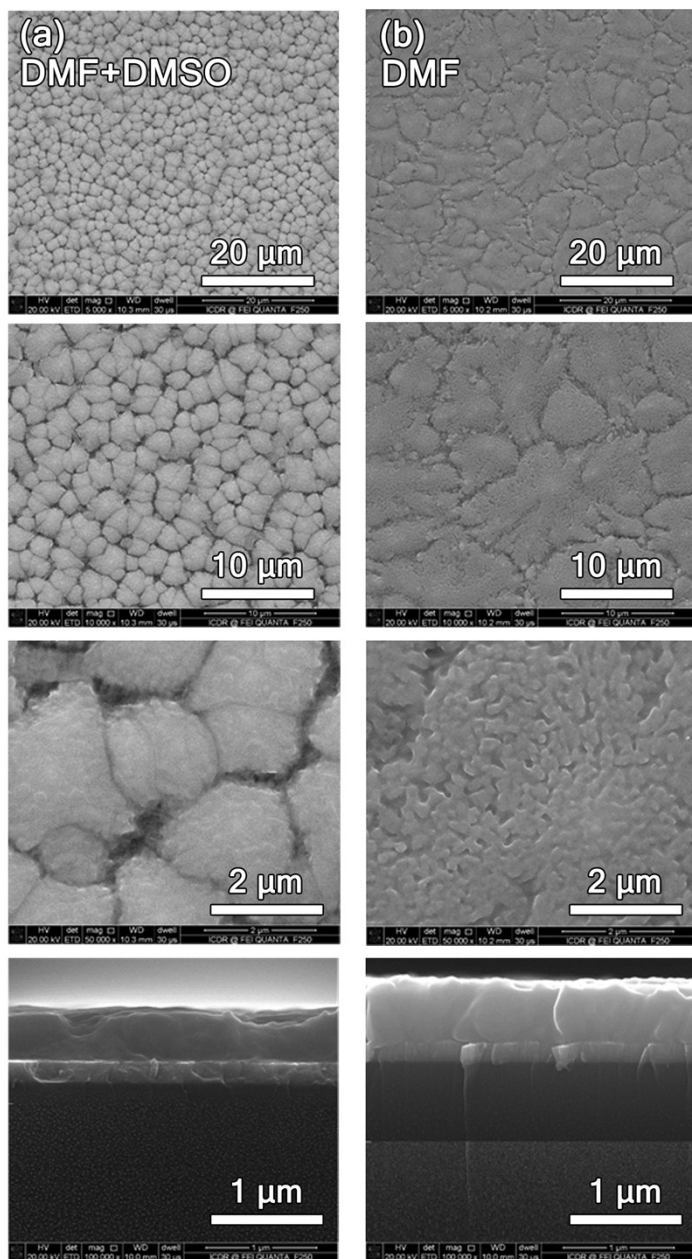


**Figure S7.** Scanning electron microscopy (SEM) images (top view and cross section) of thin films of **AgBiI<sub>4</sub>**. (a) Using dehydrate DMF/DMSO as the solvent, films with small grains of 2 μm size and wide boundary were obtained. (b) Using DMF as the solvent, films with much large grains of 10 μm size and narrow boundaries formed. Cross section views show the film thickness of about 400 nm.

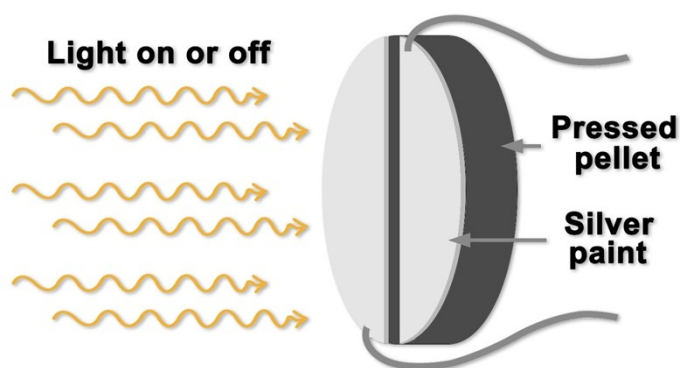


**Figure S8.** Scheme of photo-response test device.

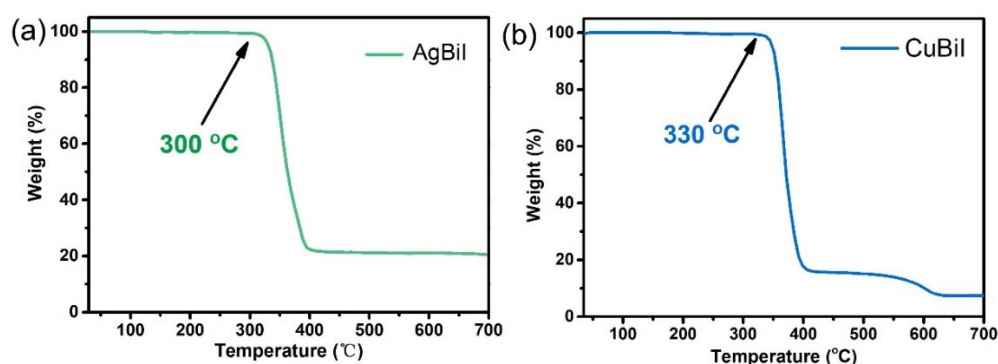


**Figure S9.** Thermogravimetric analyses (TGA) of **AgBiI** (a) and **CuBiI** (b) at a scan rate of 10 °C/min. **AgBiI** shows first obvious mass loss at 300 °C (a) and **CuBiI** shows first obvious mass loss at 330 °C (b).

Reference:

- [1] Sheldrick G. A Short History of Shelx [J]. *Acta Crystallographica Section A*, 2008, 64(1): 112-122.
- [2] Radjenović D, B S, B R, et al. The Effect of Grinding on the Apparent Colour of the Powder [J]. *American Journal of Engineering Research (AJER)*, 2018, 7(12): 97-100.
- [3] Prishivalko A P. Optimization of the Covering Power and Coloristic Properties of Pigmented Coatings on the Basis of a Four-Flux Approximation of Radiation Transport Theory [J]. *Journal of Applied Spectroscopy*, 1996, 63(5): 675-683.
- [4] Elias M. Relationship between the Size Distribution of Mineral Pigments and Color Saturation [J]. *Appl Opt*, 2011, 50(16): 2464-2473.
- [5] Gueli A M, Bonfiglio G, Pasquale S, et al. Effect of Particle Size on Pigments Colour [J]. *Color Research & Application*, 2017, 42(2): 236-243.
- [6] Connor B A, Leppert L, Smith M D, et al. Layered Halide Double Perovskites: Dimensional Reduction of Cs<sub>2</sub>agbibr<sub>6</sub> [J]. *Journal of the American Chemical Society*, 2018, 140(15): 5235-5240.
- [7] Perdew J P, Burke K, Ernzerhof M. Generalized Gradient Approximation Made Simple [J]. *Physical Review Letter*, 1996, 77(18): 3865--3868.
- [8] Monkhorst H J, Pack J D. Special Points for Brillouin-Zone Integrations [J]. *Physical Review B*, 1976, 13(12): 5188-5192.